Validation of ray and wave theoretical travel times in heterogeneous random media

Hsin-Ying Yang and Shu-Huei Hung
Department of Geosciences, National Taiwan University, Taipei, Taiwan

Received 2 June 2005; revised 4 August 2005; accepted 2 September 2005; published 18 October 2005.

[1] We investigate the validity of three theories of seismic tomography by numerical comparison of cross-correlation travel time shifts of acoustic waves with their theoretical predictions in 3-D heterogeneous random media. Whenever the characteristic heterogeneity scale length is shorter than half of the first Fresnel zone width, ray-theoretical travel times yield large discrepancies from the cross-correlation measurements. Born-Fréchet kernel theory is valid for small-scale structures but restricted to weak velocity perturbations. With increasing perturbation strength, neglecting the nonlinearity due to wave path bending in linearized ray and Born theories is no longer eligible. General ray theory accounts for the detour least-time paths in strongly heterogeneous media, which prominently improves the predicted travel times for intermediate to large scale velocity variations. **Citation:** Yang, H.-Y., and S.-H. Hung (2005), Validation of ray and wave theoretical travel times in heterogeneous random media, *Geophys. Res. Lett.*, *32*, L20302, doi:10.1029/2005GL023501.

1. Introduction

[2] Up-to-date seismic tomographic models mainly rely on ray theory or Born-Fréchet kernel theory (BKT) which translates body wave travel time anomalies into three-dimensional (3-D) aspherical velocity variations within the earth [*Grand et al.*, 1997; *Montelli et al.*, 2004]. From a ray-theoretical point of view, a seismic wave only probes the structure right on an infinitely-thin geometrical ray. Linearized ray theory (LRT) assumes that a seismic travel time shift is unchanged to first order for infinitesimally small variation in ray path and thus expressed as a line integral of slowness perturbations along the ray in a spherical earth, while general ray theory (GRT) accounts for nonlinear ray bending and evaluates the travel time along the exact least-time path in a 3-D earth model. Both theories, strictly limited to infinite-frequency waves, yield accurate travel time predictions only for the medium having smooth and large-scale velocity variation. In fact, interference of the scattered waves through heterogeneity among different frequencies renders the travel time of a broadband seismic wave sensitive to off-path structure. Recent development in finite-frequency Born theory has considered the effects of wave diffraction and scattering upon the travel time shift measured by cross-correlation of a body wave arrival with its spherical-earth synthetics [*Dahlen et al.*, 2000; *Zhao et al.*, 2000]. The resulting 3-D kernel expressing the *P* or *S* wave travel time sensitivity is identically zero everywhere along the unperturbed ray; the strong sensitivity is rather confined within the fringe of a banana-shaped region surrounding the turning ray [*Hung et al.*, 2000]. *Baig et al.* [2003] compared cross-correlation measured travel times of scalar waves in 3-D random media with the predictions from LRT and BKT. In this study, we extend the travel time comparisons in strongly heterogeneous media and address the validity of the three theories for the basis of essentially all current seismic travel time tomography.

0094-8276/05/2005GL023501

2. Acoustic Wave Propagation in Random Media

[3] We analyze the travel times of acoustic waves in a 3-D Cartesian heterogeneous medium relative to those in a homogeneous background medium, analogous to the travel times of the first compressional or shear wave arrivals relative to those in the radially symmetric Earth model. The model adopted in the numerical experiment of acoustic wave propagation is the cubic box of a dimension of $7650 \times 7650 \times 7650$ km^3 discretized on a grid of $256 \times 256 \times 256$ points. The spatial velocity variation is built on a constant wave speed ($c = 8$ km/s) superimposed with random perturbations (δc) that have the Gaussian autocorrelation function [*Sato and Fehler*,1997],

$$R(r) = \varepsilon^2 \exp\left(-r^2/a^2\right), \tag{1}$$

where r is the distance between any two points in the medium, $\varepsilon = \sqrt{\langle \delta c^2 \rangle}/c$ is the root-mean-square of fractional

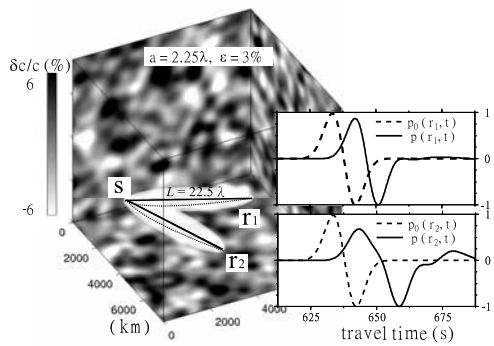

Figure 1. A Gaussian random medium with $a = 450$ km and $\varepsilon = 3\%$. The white isosurfaces depict the volumes of the Born kernels of the finite-frequency travel time shifts at two receivers $\mathbf{r}_1$ and $\mathbf{r}_2$ with the distance $L = 4500$ km from the source **s**. The solid and dashed lines indicate the straight and bending paths assumed in linearized and general ray theory, respectively. Inset on the right displays the perturbed (p) and unperturbed (p_0) pressure waveforms for cross-correlation measurements, denoted by the solid and dashed lines.

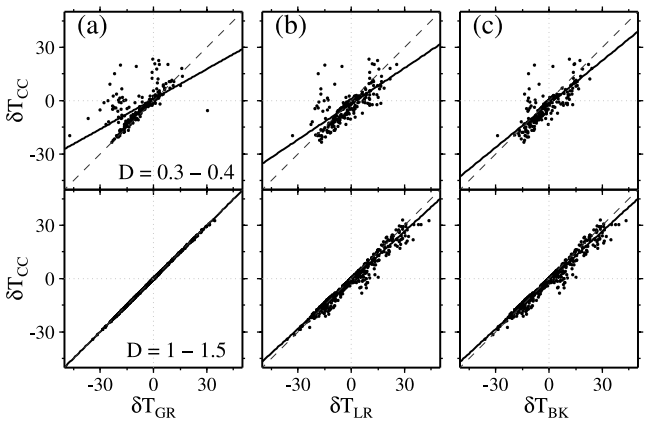

Figure 2. Scatterplot comparison of the cross-correlation measurements, δT_{CC}, with the theoretical predictions from (a) general ray theory (δT_{GR}), (b) linearized ray theory (δT_{LR}), and (c) Born kernel theory (δT_{BK}) for $\varepsilon = 6\%$. The top and bottom rows present the travel time data with $D = 0.3-0.4$ and $1-1.5$, respectively. The solid and dashed lines show the lines best fitting to the compared data and the lines of unity slope, respectively.

velocity perturbation that measures the strength of velocity heterogeneity, and a is the correlation distance that characterizes the scale length of 3-D velocity variation. Figure 1 shows the variation in $\delta c/c$ for a Gaussian random medium with $\varepsilon = 3\%$ and $a = 450$ km.

[4] We obtain ground-truth wave fields of velocity and pressure response, $p(\mathbf{x}, t)$, by solving the governing equation of acoustic wave propagation in 3-D heterogeneous media using a numerical pseudospectral method [*Hung and Forsyth*, 1998]. The simulated pressure pulse excited by an explosive point source situated at one near corner grid of the medium has a Gaussian time duration with a dominant period of $\tau = 25$ s, equivalent to the characteristic wavelength of $\lambda = 200$ km (Figure 1). The synthetic pressure seismograms for travel time measurements are computed at a number of receivers $\mathbf{r}$ with different azimuths and straight-line distances L from the source $\mathbf{s}$, ranging from 2.5λ to 30λ. See Figure A1 in the auxiliary materials[1] for the configuration of source-receiver geometry.

3. Travel Times

3.1. Cross Correlation Travel Times

[5] The ground-truth travel time shift, δT_{CC}, is determined from the time lag by which the homogeneous unperturbed pulse, $p_0(\mathbf{x}, t)$, must be shifted relative to the heterogeneous perturbed pulse, $p(\mathbf{x}, t)$, leading to a maximum correlation,

$$\int_{t_1}^{t_2} p_0(\mathbf{x}, t - \delta T_{CC})\, p(\mathbf{x}, t)\, dt = \text{maximum}. \tag{2}$$

With the increase in L and ε, synthetic seismograms can be severely contaminated by multipathed later-arriving energy. They may also suffer a phase shift from a caustic encounter which induces a change of the pulse shape. We therefore objectively select pairs of the perturbed and unperturbed seismograms whose cross-correlation coefficients are higher than the acceptance threshold of 0.90 for travel time measurements. The choice of the optimal threshold value is purely empirical. We vary the correlation coefficient threshold from 0.76 to 0.97, which reveals no significant difference for later comparison. Besides, all the acceptance percentages appear to decline rapidly beyond the critical distance, $L \geq 1.12\varepsilon^{-2/3}a$, associated with the probable appearance of the first caustic [*Spetzler and Snieder*, 2001] (Figure A2).

3.2. Ray Theoretical Travel Times

[6] Ray theory is regarded as an infinite-frequency asymptotic approximation to the full wave equation. In such limit, a finite-frequency wave travels along an imaginary minimum-time ray dictated by Fermat's principle. The exact ray-theoretical travel time shift, δT_{GR}, is the difference in travel times between $\mathbf{s}$ and $\mathbf{r}$ in a heterogeneous and homogeneous medium,

$$\delta T_{GR} = \int_{\mathbf{s}}^{\mathbf{r}} \frac{dl}{c + \delta c} - \int_{\mathbf{s}}^{\mathbf{r}} \frac{dl}{c}, \tag{3}$$

where the unadornment and adornment on an integral represent the fastest traveling route in the heterogeneous medium and the straight-line path in the homogenous medium, respectively. We employ a pseudo-bending approach for 3-D ray tracing to seek the least-time path between two points [*Um and Thurber*, 1987; *Zhao and Hasegawa*, 1993]. If $\delta c \ll c$, the high-order travel time perturbations can be ignored to yield a first-order travel time shift, δT_{LR},

$$\delta T_{LR} = -\int_{\mathbf{s}}^{\mathbf{r}} \frac{\delta c}{c^2}\, dl. \tag{4}$$

3.3. Born Theoretical Travel Times

[7] Considering the fact that a finite-frequency wave has 3-D broad off-path sensitivity, the Born theoretical travel time shift, δT_{BK}, is expressed as a volume integral [*Dahlen et al.*, 2000],

$$\delta T_{BK} = \iiint_{\oplus} K(\mathbf{x})(\delta c/c)\, d^3\mathbf{x}, \tag{5}$$

over the entire space $\oplus$ where δc is nonzero. The 3-D kernel, $K(\mathbf{x})$, represents the finite-frequency sensitivity that relates a cross-correlation travel time shift to the spatial variation in fractional wave speed perturbation, $\delta c/c$. Figure 1 illustrates the Born kernels and the bending and straight ray paths for two cross-correlation measured travel time shifts at the distance $L = 22.5\lambda$ in a Gaussian random medium with $\varepsilon = 3\%$ and $a = 2.25\lambda$. The numerical ground-truth pressure seismograms in the heterogeneous and homogeneous medium are shown in the inset plot on the right.

4. Travel Time Comparison

[8] In the forward modeling experiments, we test a broad range of characteristic parameters for the Gaussian random media; the scale length a varies from 0.75λ to 4.5λ with increments of 0.75λ and the heterogeneity strength ε varies from 1% to 10% with increments of 1%. In Figure 2 we present the scatterplot comparison of the cross-correlation

[1] Auxiliary material is available at ftp://ftp.agu.org/apend/gl/2005GL023501.

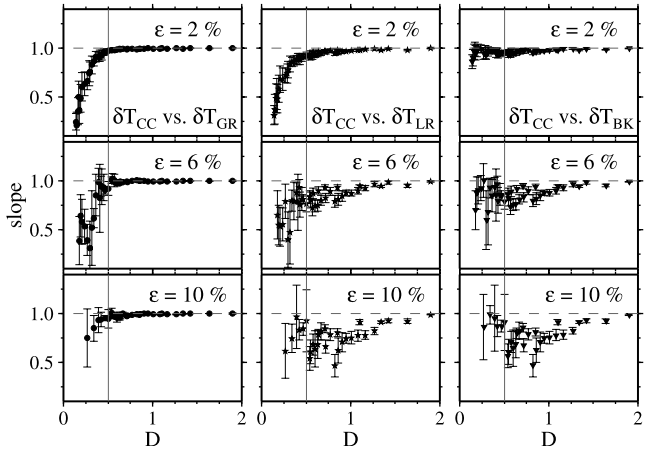

Figure 3. Scatterplot slopes of the best-fitting lines and their 95% confidence intervals versus D for ε = 2%, 6%, and 10%. The plots on the left, middle, and right columns show the slopes for cross correlation measurements, δT_{CC}, versus theoretical predictions, δT_{GR}, δT_{LR}, and δT_{BK}, respectively. All the slopes decreases rapidly for $D < 0.5$ marked by the dotted lines.

measurements versus theoretical travel time shifts for $a/\sqrt{\lambda L}$ = 0.3–0.4 and 1–1.5 and ε = 6%. The ratio of the correlation length, a, to the maximum width of the first Fresnel zone, $\sqrt{\lambda L}$, henceforth called D or the doughnut-hole parameter, acts as a critical parameter to assess the efficacy of ray theory, based on the degree to what a velocity anomaly can be hidden within the hole of low sensitivity of a 3-D banana-doughnut kernel [*Hung et al.*, 2001; *Baig et al.*, 2003].

[9] Provided that all the dots in the scatterplot lie on a straight line of unity slope and zero intercept, the theory being tested would ideally interpret ground-truth finite-frequency travel times. In the weakly heterogeneous medium ($\varepsilon \leq 3\%$), BKT is capable of modeling cross-correlation measured travel times extremely well for all the scale lengths and propagation distances. With the decreasing a and increasing L, both ray theories tend to overpredict δT_{CC} for small D as manifested by the more scattered data and reduction in the linear regression slope. Moreover, the first-order approximation applied to LRT and BKT no longer gives reliable travel time predictions for strong heterogeneity ($\varepsilon > 3\%$). General ray-theoretical travel times, on the other hand, incorporate higher-order fluctuations associated with ray bending and are in good accord with the cross-correlation measurements for $D \geq 0.5$.

[10] Figure 3 plots the best-fitting slopes and their 95% confidence intervals for all the computed travel time data versus the doughnut-hole parameter D. For the smooth and weak heterogeneity ($D \geq 0.5$ and $\varepsilon \leq 3\%$), the linearization and infinite-frequency limit are pertinent approximations; all the theories interpret the ground-truth measurements equally well. Nonetheless, finite-frequency waves at distant propagation naturally undergo the diffractive healing process that progressively flattens the rippled wavefronts and leads to smaller magnitudes of measured travel time shifts for $D < 0.5$. Ray-theoretical travel times neglect this wavefront healing effect and the best-fitting slopes readily fall below unity. Besides, the slopes obtained from LRT and BKT are somewhat less than unity even for $D > 1$. The slope deviation is particularly evident for large ε and attributed to the nonlinear travel time fluctuations due to the bending of wave paths.

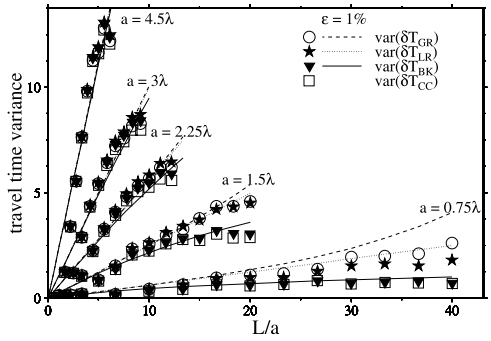

Figure 4. Travel time variances versus the dimensionless distance L/a. The circle, star, triangle and square symbols indicate the variances of the travel time shifts at fixed a and L computed by general and linearized ray theory, Born theory, and cross correlation measurements, respectively. The analytical variances derived from Born theory and ray theory at first and second order are shown by the solid, dotted and dashed lines, respectively.

[11] *Gudmundsson et al.* [1990] estimated the variances of global ISC travel time data and inferred the scale length and strength of mantle heterogeneity based on the ray-theoretical interpretation of Gaussian-medium variances. However, not only does wavefront healing result in the reduction in slope but lowers the finite-frequency travel time variances. In Figure 4 we show the variances of the theoretical and measured travel time shifts at every fixed a and L for ε = 1% versus the dimensionless distance L/a. The figure also presents the analytical variances of first and second-order ray theoretical and Born theoretical travel time shifts in Gaussian media given by *Iooss et al.* [2000] and *Baig and Dahlen* [2004], respectively. The likely sampling bias in travel time data at large L due to finite modeling space may cause the numerically-computed variances to fall off from the analytical values at the largest L for $a \geq 2.25\lambda$. Overall, the variances of cross-correlation travel time shifts are comparable to the finite-frequency Born theoretical variances but clearly less than the ray-theoretical ones at large L/a.

5. Discussion and Conclusions

[12] In essence, seismic rays are preferentially bent toward the high-velocity region so that the propagating wave speed is apparently faster than the mean velocity of

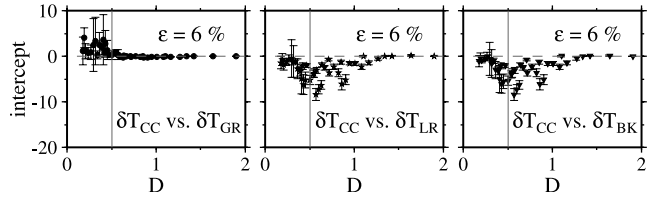

Figure 5. Scatterplot intercepts on the vertical axis of the best-fitting lines and their 95% confidence intervals versus D for ε = 6% See Figure 3 for detailed explanations.

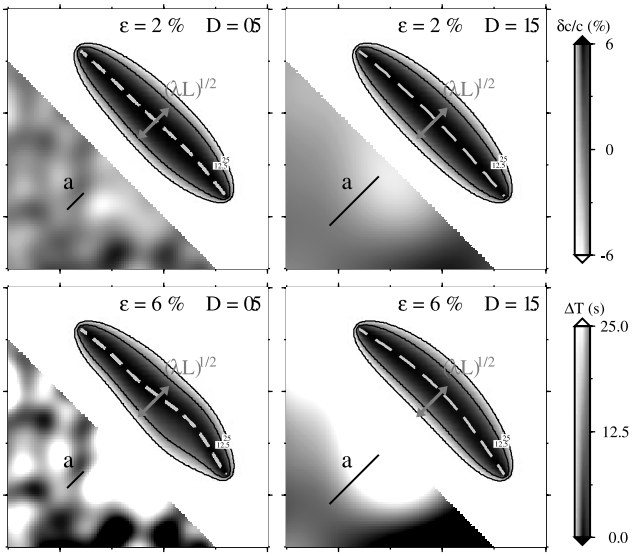

Figure 6. The Fresnel zones outlined by the additional travel time $\Delta T(\mathbf{x}) \leq 25$ s taken by a detour ray through a point scatterer **x** in random media. The top row depicts the Fresnel zones with $D = 0.5$ and 1.5 for $\varepsilon = 2\%$, while the bottom row depicts those with the same D for $\varepsilon = 6\%$. The arrows indicate the cross-path extent of the 3-D Born kernels on the midpoints of the straight rays, approximately equal to the maximum width of the first Fresnel zone, $\sqrt{\lambda L} \sim$ 900 km. Inset images on the lower left corner show the RMS of fractional velocity perturbations ε with the correlation lengths a indicated by the solid lines. See color version of this figure in the HTML.

the medium. [e.g., *Roth et al.*, 1993]. This velocity shift phenomenon theoretically related to the second order travel time fluctuations remains unaccounted for in LRT and BKT and results in the deviation of the intercepts of the scatterplot best fitting lines vertically below zero [*Baig et al.*, 2003]. Whereas GRT integrates the travel times along the exact bending trajectories of the fastest paths in the heterogeneous media, the resulting intercepts for $D \geq 0.5$ show no discernible departure from zero (Figure 5).

[13] Inasmuch as the waveforms contaminated by multiple scattered and/or multipathed arrivals are mostly excluded from cross correlation measurements, ray bending is a major cause for the deviation of linearized theoretical predictions from ground-truth travel times in strongly heterogeneous media. To illustrate the potential effect of ray bending upon the Born kernels for different ε and D, in Figure 6 we depict the approximate Fresnel zone defined as the volume sampled by every singly scattered wave through a point heterogeneity **x** that takes extra travel time $\Delta T(\mathbf{x})$ less than the dominant period $\tau = 25$ s of the unscattered wave [e.g., *Pulliam and Snieder*, 1998]. As the rays for $\varepsilon = 2\%$ at either small or large D values are only deviated slightly from the straight-line routes in the homogeneous medium, the corresponding Fresnel zones more or less resemble the ellipsoid-shaped kernels with symmetry to the source-to-receiver rays. In contrast, strong velocity gradients for $\varepsilon = 6\%$ result in severe ray bending and deform the Fresnel zones asymmetrically. Whether these bending Fresnel zone volumes truly represent the sensitivity regions of finite-frequency travel times in general 3-D media is beyond the scope of the current study and worth future investigation.

[14] To conclude, we have shown by numerical validation experiments that, to model finite-frequency travel times accurately in the medium with strong ($\varepsilon > 3\%$) and rough ($D < 0.5$) heterogeneity, the effects of wavefront healing and wave path bending have to be considered simultaneously. In local, regional, and even global tomography where the seismic-imaging structures often have large lateral velocity variations over 4% and scale lengths on the order of a few to tens of kilometers less than half of the Fresnel zone width, none of up-to-now theories enables us to resolve robust small-scale heterogeneity in deep earth. To overcome the theoretical weaknesses of linearization and infinite-frequency limitations, a nonlinear, finite-frequency theory that efficiently computes 3-D sensitivity kernels of seismic travel times is of great importance for developing the next generation high resolution earth tomographic models.

[15] **Acknowledgments.** We thank two anonymous reviewers for helpful comments. We also thank Adam Baig for the code to generate Gaussian random media and Dapeng Zhao for the 3-D ray tracing program. Numerical simulations were conducted on a 16-node PC cluster at the Department of Geosciences of National Taiwan University (NTU), funded by National Science Council (NSC) of Taiwan and NTU. This research was supported by NSC under grants NSC91-2611-M-002-025 and NSC91-2119-M-002-027.

References

Baig, A. M., and F. A. Dahlen (2004), Statistics of traveltimes and amplitudes in random media, *Geophys. J. Int.*, *158*, 187–210.

Baig, A. M., F. A. Dahlen, and S.-H. Hung (2003), Traveltimes of waves in three-dimension random media, *Geophys. J. Int.*, *153*, 467–482.

Dahlen, F. A., S.-H. Hung, and G. Nolet (2000), Fréchet kernels for finite-frequency traveltimes—I. Theory, *Geophys. J. Int.*, *141*, 157–174.

Grand, S. P., R. D. van der Hilst, and S. Widiyantoro (1997), Global seismic tomography: A snapshot of convection in the Earth, *GSA Today*, *7*, 1–7.

Gudmundsson, O., J. H. Davies, and R. W. Clayton (1990), Stochastic analysis of global traveltime data: mantle heterogeneity and random error in the ISC data, *Geophys. J. Int.*, *102*, 25–43.

Hung, S.-H., and D. W. Forsyth (1998), Modelling anisotropic wave propagation in oceanic inhomogeneous structures using the parallel multidomain pseudo-spectral method, *Geophys. J. Int.*, *133*, 726–740.

Hung, S.-H., F. A. Dahlen, and G. Nolet (2000), Fréchet kernels for finite-frequency traveltimes—II. Examples, *Geophys. J. Int.*, *141*, 175–203.

Hung, S.-H., F. A. Dahlen, and G. Nolet (2001), Wavefront healing: A banana-doughnut perspective, *Geophys. J. Int.*, *146*, 289–312.

Iooss, B., P. Blanc-Benon, and C. Lhuillier (2000), Statistical moments of travel times at second order in isotropic and anisotropic random media, *Waves Random Media*, *10*, 381–394.

Montelli, R., G. Nolet, G. Masters, F. A. Dahlen, E. R. Engdahl, and S.-H. Hung (2004), Finite-frequency tomography reveals a variety of plumes in the mantle, *Science*, *303*, 338–343.

Pulliam, J., and R. Snieder (1998), Ray perturbation theory, dynamic ray tracing and the determination of Fresnel zones, *Geophys. J. Int.*, *135*, 463–469.

Roth, M., G. Müller, and R. Snieder (1993), Velocity shift in random media, *Geophys. J. Int.*, *115*, 552–563.

Sato, H., and M. C. Fehler (1997), *Seismic Wave Propagation and Scattering in the Heterogeneous Earth*, Springer, New York.

Spetzler, J., and R. Snieder (2001), The formation of caustics in two- and three-dimensional media, *Geophys. J. Int.*, *144*, 175–182.

Um, J., and C. Thurber (1987), A fast algorithm for two-point seismic ray tracing, *Bull. Seismol. Soc. Am.*, *77*, 972–986.

Zhao, D., and A. Hasegawa (1993), P wave tomographic imaging of the crust and upper mantle beneath the Japan islands, *J. Geophys. Res.*, *98*, 4333–4353.

Zhao, L., T. H. Jordan, and C. H. Chapman (2000), Three-dimensional Fréchet differential kernels for seismic delay times, *Geophys. J. Int.*, *141*, 558–576.

S.-H. Hung and H.-Y. Yang, Department of Geosciences, National Taiwan University, Taipei, 106, Taiwan. (shung@ntu.edu.tw; r92224204@ntu.edu.tw)